

A comparative study of model approximation methods applied to economic MPC

Zhiyinan Huang^{a,*}, Qinyao Liu^{a,b,*}, Jinfeng Liu^{a,†}, Biao Huang^a

^aDepartment of Chemical & Materials Engineering, University of Alberta,
Edmonton, AB T6G 1H9, Canada

^bSchool of Internet of Things Engineering, Jiangnan University,
Wuxi 214122, PR China

Abstract

Economic model predictive control (EMPC) has attracted significant attention in recent years and is recognized as a promising advanced process control method for the next generation smart manufacturing. It can lead to improving economic performance but at the same time increases the computational complexity significantly. Model approximation has been a standard approach for reducing computational complexity in process control. In this work, we perform a study on three types of representative model approximation methods applied to EMPC, including model reduction based on available first-principle models (e.g., proper orthogonal decomposition), system identification based on input-output data (e.g., subspace identification) that results in an explicitly expressed mathematical model, and neural networks based on input-output data. A representative algorithm from each model approximation method is considered. Two processes that are very different in dynamic nature and complexity were selected as benchmark processes for computational complexity and economic performance comparison, namely an alkylation process and a wastewater treatment plant (WWTP). The strengths and drawbacks of each method are summarized according to the simulation results, with future research direction regarding control oriented model approximation proposed at the end.

1 Introduction

In the past decade, economic model predictive control (EMPC) is recognized as a promising advanced process control and decision-making framework for the next generation smart manufacturing [1]. However, solving the EMPC optimization problem often leads to significant computational load,

*Both Zhiyinan Huang and Qinyao Liu are co-first authors and have contributed equally to the work. Qinyao Liu focused more on traditional model approximation and identification while Zhiyinan Huang focused more on explicitly-expressed neural network and optimization.

[†]Corresponding author: J. Liu. Tel: +1-780-492-1317. Fax: +1-780-492-2881. Email: jinfeng@ualberta.ca.

especially in large-scale systems [1, 2]. Model approximation has been considered to be an effective way to reduce the computational burden and improve the applicability of EMPC for large-scale processes [3]. It aims to approximate the original system with an appropriately simplified model that captures the main dynamics of the original system. The popular methods for model approximation can be broadly classified into three categories: model reduction based on first-principle models (e.g., proper orthogonal decomposition) [4], traditional data-based system identification (e.g., subspace identification) [5, 6, 7, 8], and machine-learning-based model identification [9].

Model reduction techniques require the existence of a (typically first-principle) model of the considered system [10, 11]. Many model reduction methods in this category are projection-based methods, in which the original high-order system is projected onto a lower-order reduced space [11]. Among them, the proper orthogonal decomposition (POD) is one of the most widely used methods, which is for example applied in [4] together with the discrete empirical interpolation method to solve large-scale model predictive control (MPC) problems for continuous chemical processing.

In the cases that only the input-output dataset is available, system identification techniques are frequently used to establish the mathematical model of a dynamical system [12, 13], where relatively simple models can be generated without knowledge regarding the underlying physical laws of the system. There are mainly three types of system identification methods, namely the prediction error method [14], maximum likelihood method [15], and subspace identification method [5]. Different from the first two methods that require pre-selected model structure and solving optimization problems, the subspace identification method can directly extract the state-space model from the input-output data without using optimization techniques [5, 8].

Different from system identification methods, data-driven machine-learning-based model identification typically leads to neural network (NN) models that do not have explicit mathematical expressions [9]. With the ability to acquire knowledge from the input information and remember the learning results, neural networks can approximate any continuous function according to the universal approximation theorem [16]. Much attention has been attracted to neural-network-based system modeling [17, 18] and control [19]. However, for various applications, neural networks often suffer from their black-box nature. Thus explicitly expressed NNs were proposed and applied in some areas [20].

In this work, we perform critical examination of these model approximation methods when used in conventional tracking MPC and EMPC. One representative model approximation method is selected from each of the three model approximation categories. Specifically, POD integrated with trajectory piecewise linearization (TPWL) [7], subspace identification [8], and explicitly-expressed fully connected neural network is selected for this work. Two processes that are very different

in dynamic nature and complexity are selected as benchmark processes. Conventional tracking MPC controllers and EMPC controllers designed based on the three model approximation methods are applied to the benchmark processes. The performance of the control framework is compared from different aspects, including computational complexity, tracking performance for MPC, and economic performance for EMPC.

2 Preliminaries

2.1 System description and problem formulation

In this work, we consider model approximation of nonlinear dynamical systems that can be described using the following ordinary differential equations:

$$\dot{x}(t) = f(x(t), u(t)) \quad (1a)$$

$$y(t) = g(x(t), u(t)) \quad (1b)$$

where $x \in \mathbb{R}^n$ is the state vector, $u \in \mathbb{R}^r$ is the input vector, $y \in \mathbb{R}^l$ is the output vector, f and g are nonlinear vector functions, f describes the dynamics of the system and g describes the relation of the output to the state and the input. For convenience, we will refer to the system in (1) as the *original system* in the remainder of this work.

Model approximation will be applied to either reduce the original system to a system of a lower order that approximates the dynamics of the original system with sufficient accuracy or to identify a linear or neural network model based on the input-output data of the original system. These reduced or identified models will be applied in advanced control frameworks as system constraints and their applicability and performance will be carefully examined. To be specific, conventional set-point tracking MPC and EMPC will be investigated and differences in control behaviors of these two frameworks with respect to different reduced or identified models are of our interest.

2.2 Model predictive control design

We consider a MPC formulation that tracks an optimal steady-state operating point (y_s, u_s) . The tracking MPC at a specific sampling time t_i is formulated as an optimization problem as follows:

$$\min_{u(t) \in S(\Delta)} \sum_{j=i}^{i+N-1} \left(|y(t_j|t_i) - y_s|_Q^2 + |u(t_j|t_i) - u_s|_R^2 \right) + |y(t_{k+N}|t_i) - y_s|_{P_f}^2 \quad (2a)$$

$$\text{s.t. : } \dot{x}(t) = f(x(t), u(t)) \quad (2b)$$

$$y(t) = g(x(t), u(t)) \quad (2c)$$

$$x(t_i) = \bar{x}(t_i) \quad (2d)$$

$$u(t) \in \mathbb{U} \quad (2e)$$

$$y(t) \in \mathbb{Y} \quad (2f)$$

where $S(\Delta)$ is the family of piece-wise constant function with Δ being the sampling time, N is the prediction horizon and is a finite positive integer, $y(t|t_i)$ and $u(t|t_i)$ represent the prediction of the variables at future time t made at the current time t_i . Q , R and P_f are diagonal weighting matrices, $\bar{x}(t_i)$ is the estimated or measured state vector at current time t_i , $\mathbb{U} \subset \mathbb{R}^r$ and $\mathbb{Y} \subset \mathbb{R}^l$ are compact sets. The optimization problem aims to optimize $u(t)$ from t_i to t_{i+N-1} , such that the accumulated difference between $(y(t|t_i), u(t|t_i))$ and the set-point (y_s, u_s) is minimized, which is defined by the objective function (2a). System model (2b) - (2c) are employed to predict $y(t|t_i)$ with initial condition specified by (2d). (2e)-(2f) are input and output constraints that have to be satisfied over the entire horizon N while solving the problem.

Note that when a reduced or identified model is used to design the MPC controller, the model equations (2b)-(2c) should be replaced with the reduced or identified model equations accordingly.

The optimal solution of the above optimization problem can be denoted as $u_{\text{EMPC}}^*(t|t_i)$. However, only the values at the first time instant (i.e. the current time t_i) will be applied to the system:

$$u(t) = u_{\text{EMPC}}^*(t|t_i), \quad t \in [t_i, t_{i+1}) \quad (3)$$

Regarding the optimal operating point (y_s, u_s) employed in (2a), it may be calculated through a steady-state optimization problem as shown in (4),

$$(y_s, u_s) = \min_{y, u} l_e(y, u) \quad (4a)$$

$$\text{s.t. : } \dot{x} = f(x, u) \quad (4b)$$

$$y = g(x, u) \quad (4c)$$

$$u \in \mathbb{U} \quad (4d)$$

$$y \in \mathbb{Y} \quad (4e)$$

where the objective function $l_e(y, u)$ represents an economic performance of the system.

2.3 Economic model predictive control design

As have presented in the previous section, MPC takes a two-layered design. The optimal operating point is first obtained by solving a steady-state optimization problem. A series of dynamic optimization problems that tracks the states and inputs to the optimal operating point is then proceeded along the horizon of interest. In EMPC design, these two steps are combined into a single step. The objective function used in the steady-state optimization, which is often times economic performance related, is directly employed in the dynamic optimization problems.

A basic EMPC formulation for the system described in (1) is employed in this work. EMPC is in general formulated as an optimization problem, which takes the following form at the sampling time t_i [1]:

$$\min_{u(t) \in S(\Delta)} \sum_{j=i}^{i+N-1} l_e(y(t_j|t_i), u(t_j|t_i)) \quad (5a)$$

$$\text{s.t.} \quad \dot{x}(t) = f(x(t), u(t)) \quad (5b)$$

$$y(t) = g(x(t), u(t)) \quad (5c)$$

$$x(t_i) = \bar{x}(t_i) \quad (5d)$$

$$u(t) \in \mathbb{U} \quad (5e)$$

$$y(t) \in \mathbb{Y} \quad (5f)$$

The same definitions as used in the MPC formulation are also valid for the EMPC formulation. The only difference lies in the objective function as used in (5a), where the economic performance index employed in the steady-state optimization is adapted in dynamic optimization directly.

3 Model Approximation Methods

In this section, the model approximation methods encountered in this work are briefly introduced. The characteristics of each approaches are discussed, followed by step-by-step descriptions of how the methods can be implemented.

3.1 Model reduction based on first-principle model

First, we introduce the proper orthogonal decomposition (POD) and trajectory piecewise linearization (TPWL) methods. The two methods represent the two popular approaches to reduce model complexity respectively, namely reducing the model order and mimicking complex mathematical

relationships in simpler structures (e.g. linearization). Applications of these two methods can be found in various works, for example, [7, 21] for POD and [7, 22] for TPWL. A combination of POD and trajectory piecewise linearization (TPWL) is considered in this work.

The key idea of the POD method is to obtain a projection matrix that projects the original state vector onto a lower-dimensional space. To achieve this goal, a snapshot matrix of the states X is first generated by simulating the original system with an input trajectory that ensures persistent excitation of the system. The snapshot X contains sampled system states at different time instants. Suppose that:

$$X = [x(t_1), x(t_2), x(t_3), \dots, x(t_N)] \in \mathbb{R}^{n \times N}$$

where $x(t_i)$, $i = 1, \dots, N$, is the sampled state vector at time t_i , N is the total number of samples, n is the dimension of the state vector. Note that N should be much greater than n to ensure that the snapshot captures the dynamics of the original system. After X is generated, singular value decomposition (SVD) is applied to X to obtain the following decomposition:

$$X = U\Sigma V^T \tag{6}$$

where $U \in \mathbb{R}^{n \times n}$ and $V \in \mathbb{R}^{N \times N}$ are orthogonal matrices and are referred to as the left and right singular matrix of X respectively, $\Sigma = \text{diag}^1([\sigma_1, \sigma_2, \dots, \sigma_n]) \in \mathbb{R}^{n \times N}$ is a diagonal matrix, where $\sigma_1, \dots, \sigma_n$ are the n singular values of X and are arranged in a descending order. It is noted that the greater the value of a singular value, the more important system dynamics it captures. In POD, the order of the reduced system is determined based on these singular values. It is recommended that the order k is obtained such that there is a significant drop in the singular value magnitude from σ_k to σ_{k+1} . Once k is determined, the projection matrix $U_k \in \mathbb{R}^{n \times k}$ is defined to be the first k columns of the matrix U . The reduced system state $z(t)$ has the following relationship with the original state $x(t)$:

$$x(t) = U_k z(t) \tag{7}$$

It is to be noted that although POD reduces the system order to a smaller number, the underlying calculations in general do not reduce from a numeric optimization point of view. This is because that it is in general challenging to explicitly express the reduced system for medium to large scale nonlinear systems. Thus when the original system has complex nonlinear dynamics, applying only POD to the system often does not reduce the computational complexity. A common way to deal with this problem is to simplify the mathematical complexity of the original system first, followed by applying POD on the simplified model. Readers can refer to [7] for an example application of

¹diag(v) denotes a diagonal matrix with the diagonal elements being the elements of the vector v

this approach, where POD was applied to a linear time-varying (LPV) reduced model obtained using TPWL.

Instead of linearizing at a single point, in TPWL, the original system is linearized along a typical state trajectory at multiple points. With a predetermined number of linearization points, the operating region of interest should be covered evenly by the selected linearization points. This can be achieved by the application of a distance-based algorithm which is introduced in [23]. After linearization, the linearized models at different points are combined through weighted summation to form an LPV model. The weighting function may be designed in a way such that once the state-input pair approaches one of the linearization points, the weight for the corresponding sub-model increases to one quickly.

Let us assume that there are s linearization points. The weighting function $w_i(\cdot), i = 0, \dots, s-1$ that combines the linearized models can be determined following [23]. The procedure for implementing POD with TPWL is summarized as follows[23]:

1. Run open-loop simulations using the original model and generate the snapshot matrix X using the open-loop simulation data.
2. Based on the snapshot matrix X , calculate the projection matrix U_k as the truncated left singular matrix U_k of the snapshot matrix X following (6) and (7).
3. Based on extensive simulations of the original system, determine a representative trajectory of the system and along the trajectory, determine the s linearization points based on the distance-dependent algorithm discussed in [23].
4. Obtain the s linearized models by linearizing the original system at each of the s linearization points.
5. Based on the s linearized models and the weighting function $w_i(\cdot), i = 0, \dots, s-1$, the LPV model that combines all the linearized models takes the following form:

$$\dot{x} = \sum_{i=0}^{s-1} w_i(x)(A_i(x - x_i) + B_i(u - u_i) + f(x_i, u_i)) \quad (8a)$$

$$y = \sum_{i=0}^{s-1} w_i(x)(C_i(x - x_i) + D_i(u - u_i) + g(x_i, u_i)) \quad (8b)$$

where x_i, u_i for $i = 0, 1, \dots, s-1$ represents the linearization points, A_i, B_i, C_i, D_i are the partial derivatives $\frac{\partial f}{\partial x}, \frac{\partial f}{\partial u}$ and $\frac{\partial g}{\partial x}, \frac{\partial g}{\partial u}$ evaluated at the linearization points, respectively.

6. Use the projection matrix U_k to project the high-order LPV model (8) onto a lower-order state-space as follows:

$$\dot{z} = \sum_{i=0}^{s-1} w_i(U_k z) U_k^T [(A_i(U_k z - U_k z_i) + B_i(u - u_i) + f(U_k z_i, u_i))] \quad (9a)$$

$$y = \sum_{i=0}^{s-1} w_i(U_k z) (C_i(U_k z - U_k z_i) + D_i(u - u_i) + g(U_k z_i, u_i)) \quad (9b)$$

where z_i represents the i th reduced linearization point.

3.2 Subspace model identification

When the first-principle model is not available, model identification based on input-output data of the system is the common approach for model development. There are many different model identification algorithms. In this work, we will focus on subspace identification. Unlike other traditional identification methods that require predetermined model structure and order, subspace identification has the unique property that the model can be identified with only the input-output dataset. Furthermore, the subspace method is purely linear-algebra-based and does not involve solving optimization problems [5].

The subspace identification method leads to a discrete-time linear time-invariant (LTI) state-space model in the following form:

$$z_{k+1} = Az_k + Bu_k, \quad (10a)$$

$$y_k = Cz_k + Du_k, \quad (10b)$$

where $z_k \in \mathbb{R}^s$, $u_k \in \mathbb{R}^r$ and $y_k \in \mathbb{R}^l$ are the state vector, input vector and output vector, respectively, $A \in \mathbb{R}^{s \times s}$, $B \in \mathbb{R}^{s \times r}$, $C \in \mathbb{R}^{l \times s}$ and $D \in \mathbb{R}^{l \times r}$ are system matrices. The model is obtained by first calculating the extended observability matrix of the system using techniques such as oblique projection, from which matrices C and A can be calculated. Matrices B and D can then be obtained using least square methods.

The subspace identification algorithm can be summarized as follows[5]:

1. Calculate the oblique projection of Y_f along the row space of U_f on to the row space of Z_p , where Y_f , U_f , and Z_p are the block Hankel matrix consists of future outputs, future inputs and past inputs and outputs ($Z_p = [U_p^T \ Y_p^T]^T$, U_p and Y_p are the Hankel matrix consist the past input and outputs) respectively.

$$O_i = Y_f /_{U_f} Z_p \quad (11)$$

2. Perform SVD on O_i :

$$O_i = \begin{pmatrix} U_1 & U_2 \end{pmatrix} \begin{pmatrix} S_1 & 0 \\ 0 & 0 \end{pmatrix} \begin{pmatrix} V_1^T \\ V_2^T \end{pmatrix}, \quad (12a)$$

$$\Gamma_i = U_1 S_1^{1/2}, \quad (12b)$$

$$X_f = \Gamma_i^\dagger O_i, \quad (12c)$$

where the columns of $(U_1 \ U_2)$ are the left singular vectors of O_i , S_1 is the diagonal matrix that contains the nonzero singular values of O_i , Γ_i is the extended observability matrix, X_f is the Hankel matrix that consists the future states, $(\cdot)^\dagger$ denotes the Moore-Penrose pseudo-inverse of the matrix (\cdot) . The dimension s of the state is determined by the dimension of S_1 .

3. Compute the extended observability matrix Γ_i based on (12b), and the orthogonal complement of the row space of Γ_i can be calculated by $\Gamma_i^\perp = U_2^T$, where $(\cdot)^\perp$ denotes the orthogonal complement of the row space of the matrix (\cdot) .

4. Determine C as the first l rows of Γ_i , where l is the dimension of the output vector. According to the definition of Γ_i , we can find the following relation:

$$\begin{pmatrix} C \\ CA \\ CA^2 \\ \dots \\ CA^{i-2} \end{pmatrix} A = \begin{pmatrix} CA \\ CA^2 \\ CA^3 \\ \dots \\ CA^{i-1} \end{pmatrix}, \quad \underline{\Gamma}_i A = \overline{\Gamma}_i,$$

where $\underline{\Gamma}_i$ denotes Γ_i without the last l rows and $\overline{\Gamma}_i$ is Γ_i without the first l rows. Then A can be solved by $A = \underline{\Gamma}_i^\dagger \overline{\Gamma}_i$.

5. Calculate the matrix $\Gamma_i^\perp Y_f U_f^\dagger$, and construct

$$\begin{aligned} \Gamma_i^\perp Y_f U_f^\dagger &= \begin{pmatrix} M_1 & M_2 & \dots & M_i \end{pmatrix}, \\ \Gamma_i^\perp &= \begin{pmatrix} L_1 & L_2 & \dots & L_i \end{pmatrix}, \end{aligned}$$

then B and D can be solved from

$$\begin{pmatrix} M_1 \\ M_2 \\ \vdots \\ M_i \end{pmatrix} = \begin{pmatrix} L_1 & L_2 & \cdots & L_{i-1} & l_i \\ L_2 & L_3 & \cdots & L_i & 0 \\ L_3 & L_4 & \cdots & 0 & 0 \\ \cdots & \cdots & \cdots & \cdots & \cdots \\ L_i & 0 & \cdots & 0 & 0 \end{pmatrix} \begin{pmatrix} I_l & 0 \\ 0 & \underline{\Gamma_i} \end{pmatrix} \begin{pmatrix} B \\ D \end{pmatrix}$$

3.3 Neural network modeling

The last method to be introduced is to train neural networks as system models. Similar to the subspace identification method introduced in the previous section, neural network training does not require a significant amount of knowledge regarding the dynamics of the interested system. Furthermore, NNs can capture nonlinear dynamics much easier compared to the subspace identification method. According to the universal approximation theorem [24], neural networks in general are capable of approximating any function $f : \mathbb{R}^n \rightarrow \mathbb{R}^m$ with n -dimension inputs and m -dimension outputs up to some maximum error ε . In this work, fully connected neural networks with nonlinear activation functions are considered. Unlike models obtained with traditional identification methods, neural networks are often used as black-box models without explicit expressions, which could be challenging for advanced control applications. This is because many of the conventional optimization solvers require Jacobian/Hessian information of the systems, which could be computationally expensive for black-box models. In this work, NN system models are investigated in the form of basic black-boxes as well as explicitly expressed systems of equations.

A brief step-by-step procedure for identifying a NN model is outlined as follows [25]:

1. Determine the dimension of the NN input and output vectors:

$$NN_{in} \in \mathbb{R}^{N_{past} \cdot (r+l) + (N_{future}-1) \cdot r}$$

$$NN_{out} \in \mathbb{R}^{N_{future} \cdot l}$$

where N_{past} is the number of past steps considered, N_{future} is the number of future time steps to be predicted. Note that the inputs of the NN includes both system inputs and outputs from the past. Furthermore, when system output at multiple future steps are of interests, the future system inputs for the corresponding steps are as well required as NN inputs.

2. Determine the number of NN layers, the number of nodes in each layer, and the activation function to be used. Note that there are no universal rules for determining these parameters.

Users can manually do guess-and-check or use tools such as grid search.

3. Reconstruct the dataset according to the predetermined input-output dimension.
4. Identify the NN using computational tools (e.g. the state-of-the-art application program interface (API) Keras [29]).
5. Extract the trained parameters from the model.
6. Define explicit models with the trained parameters and the known NN structure. A single fully-connected NN can be defined as follows:

$$y = \sigma\left(\sum_{i=1}^{n_{node}} w_i x_i + b_i\right) \quad (13)$$

where x and y represents the input and output of the NN layer, w_i and b_i are the weighting factor and the bias for the i^{th} input, n_{node} is the number of nodes in the NN layer, $\sigma(\cdot)$ is the activation function.

In the following two sections, we consider two benchmark process examples and study the performance of the three model approximation methods when they are used in MPC and EMPC designs. The two benchmark processes are selected to be very different in scales and dynamic natures, such that the performance of the model approximation methods applied to different types of systems can be investigated and a more comprehensive comparison can be done.

4 Case Study 1: Benzene Alkylation Process

4.1 Process overview

The first benchmark process considered is a benzene alkylation process. A schematic diagram of the process is presented in Figure 1 [27]. The process considered consists of four CSTRs and a flash tank separator. Stream F_1 consist of pure benzene while streams F_2 , F_4 and F_6 consist pure ethylene. Two catalytic reactions take place in CSTR-1, CSTR-2, and CSTR-3, of which benzene (A) react with ethylene (B) and produce the desired product ethylbenzene (C) (reaction 1), while ethylbenzene further react with ethylene and produce the byproduct 1,3-diethylbenzene (D) (reaction 2). The effluent of CSTR-3 is fed to the flash tank separator, where the desired product is separated and leave from the bottom stream F_8 . On the other hand, the left-over benzene leaves the separator from the top and splits into $F_{7,1}$ and $F_{7,2}$ which goes into CSTR-4 and CSTR-1 respectively. 1,3-diethylbenzene is fed into CSTR-4 through F_{10} , where it reacts with

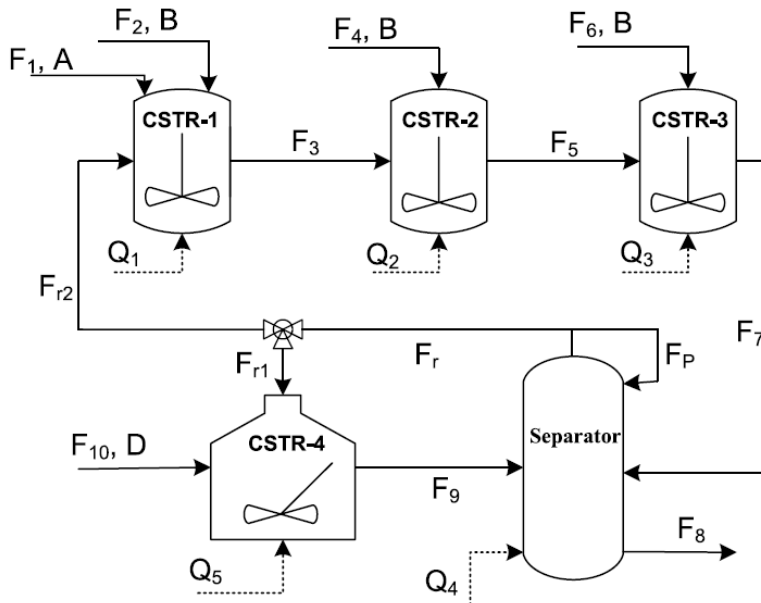


Figure 1: A schematic of the alkylation of benzene process

benzene to produce ethylbenzene under the presence of catalysts (reaction 3). All the chemicals leaving from CSTR-4 eventually goes to the separator. Each vessel has an external heat supply stream which helps to adjust the vessel temperature ($Q_1 - Q_5$).

The state variables of the process are the concentrations of the four chemical components and the temperature in each vessel. The manipulated inputs are the external heat supply and the feed stream flow rates of ethylene going into CSTR-2 and CSTR-3. Overall, the system consists of 25 states and 7 manipulated inputs. A more detailed model description with parameter values can be found in [27].

4.2 Control objective and controller setting

The control objective is to maximize the production rate of ethylbenzene while keeping the energy cost at a reasonable level. Thus the economic performance measure employed for the steady-state optimization and the EMPC controller is defined as follows:

$$l_e = -\alpha F_8 C_{C4} + \beta \sum_{i=1}^5 |Q_{is} + Q_i| \quad (14)$$

where F_8 and C_{C4} are the flow rate and ethylbenzene concentration leaving the separator respectively, Q_i represents the deviation heat inlet to vessel i with respect to the steady-state values. Q_{is} is the steady-state heat inlet for the corresponding vessel, $\alpha = 200$ and $\beta = 0.0005$ are the

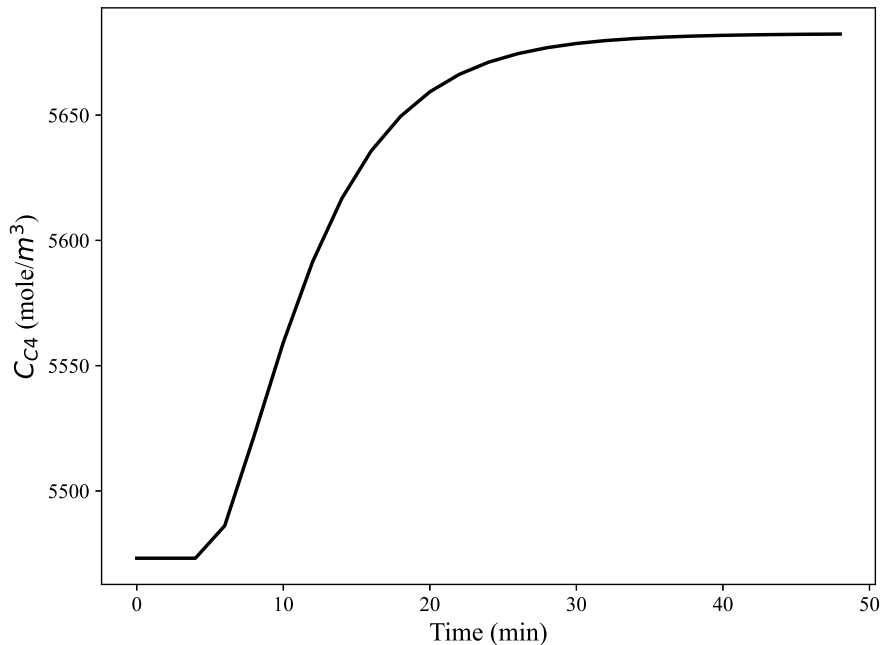


Figure 2: Step response of the alkylation process output.

weighting coefficients selected so that a fair trade-off between production rate and operating cost is established. Note that although the flow rates of ethylene feeding into CSTR-2 and CSTR-3 do not present explicitly in the objection function, the value of F_8 however depends on them.

The weighting factors used in the MPC tracking objective function (2a) were selected to be $Q = 1$, $R = \text{diag}([7.5, 5, 5, 6, 5, 4.9 \cdot 10^{-4}, 4.9 \cdot 10^{-4}])$ and $P_f = 10$, where a higher penalty was added to the terminal output to enhance convergence. For simplicity, the output vector y is C_{C4} , which is the only state appeared in (14). The observability of the system is confirmed using the PBH test along the data trajectory with the selected output. The optimal steady-state operating point $y_s = 5526$, $u_s = [1.0, 1.0, 1.0, -1.0, -0.86, 1.0, 1.0]$ is obtained by solving the steady-state optimization (4). The input vector and the output are bounded based on physical properties of the process.

$$\mathbb{U} = \{u | \underline{u} \leq u \leq \bar{u}\} \quad (15a)$$

$$\mathbb{Y} = \{y | y \geq 0\} \quad (15b)$$

where \underline{u} and \bar{u} are the upper and lower bound of the input vector. The exact values of \underline{u} and \bar{u} can be found in [27].

The controller sampling time is 2 minutes, and the prediction horizon is $N = 15$. The two

parameters are picked based on the output response (Figure 2) with a unit step change in the input vector u . As presented in Figure 2, the major dynamics of the system can be captured in the 30-minute window defined by the sampling time and prediction horizon.

4.3 Data generation and model approximations

All the methods discussed in section 3 require the generation of a dataset that can represent the dynamics of the original process. Given that the considered alkylation process is nonlinear, multi-level input signals are used as the inputs to the process for input-output data generation. Open-loop simulations are carried out with the multi-level inputs applied to the original nominal system model. For consistency, one dataset is generated and is used for all the model approximation methods.

Figure 3 shows a portion of the input signal employed for the alkylation process and the corresponding output response. Note that the input signal is normalized with respect to the steady-state.

At a given time step k , each element in the input vector u randomly takes a value from a predetermined set \mathbb{U}_d and hold onto that value until time $(k + n_{hold})$. Note that $n_{hold} \in \mathbb{I}_a^b = \{a, a + 1, \dots, b\}$, where \mathbb{I}_a^b is an integer set with a and b being the lower and upper bounds. At time step $k + n_{hold}$, the element values of the input vector u will be reselected from \mathbb{U}_d .

The sets \mathbb{U}_d and \mathbb{I}_a^b can be designed base on the dynamics of the system such that the frequency and magnitude of the step changes can excite the system properly. If only the upper and lower bounds of the input vectors are included in \mathbb{U}_d , the input signal becomes a pseudorandom binary sequence (PRBS). For the alkylation process to be specific, the set \mathbb{U}_d was designed to have five elements which were obtained by equally splitting the input domain \mathbb{U} :

$$\mathbb{U}_d = \{\underline{u}, \underline{u} + \frac{\delta_u}{4}, \underline{u} + \frac{\delta_u}{2}, \underline{u} + \frac{3\delta_u}{4}, \bar{u}\}, \delta_u = \bar{u} - \underline{u}$$

Taking into account of the rapid ongoing chemical reactions in the alkylation process, the integer set \mathbb{I}_a^b , $a = 10, b = 16$ was used. This means that the input will hold onto the same values for 20 to 32 minutes before the next set of values can be picked from \mathbb{U}_d .

To ensure reasonable results from the considered methods, 5000 data points were generated. The reduced model order k was determined by guess and check, where reduced models of different orders were generated based on the original model first and open-loop prediction performances were checked and compared through a step test. The model order that gives a satisfying balance between prediction accuracy and model order was selected and employed for the TPWL-POD models.

Data scaling and reconstructions are required for NN identification such that the preselected input-output dimension is satisfied. The Python library Keras [29] was used to identify a fully-

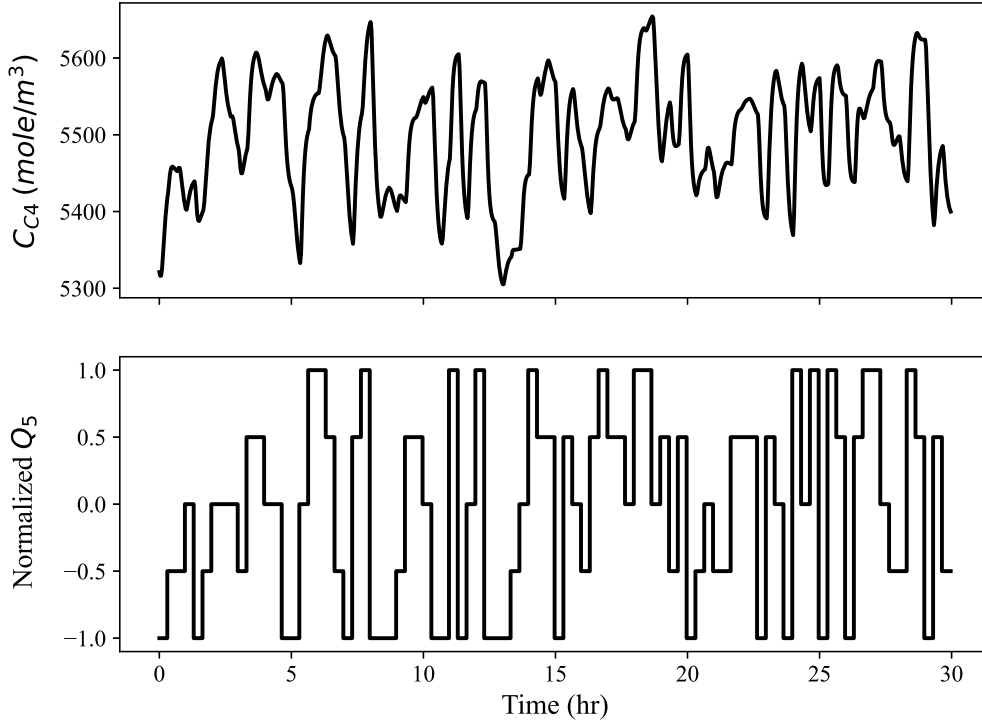


Figure 3: Multi-level input and the corresponding output response.

connected NN model which takes the form of:

$$f : \mathbb{R}^{359} \rightarrow \mathbb{R}^{15}$$

where $359 = 30 \times 8 + 14 \times 7$, 8 is the number of inputs plus outputs, 30 is the number of past data points used, 7 is the number of inputs, 14 is the number of future inputs encountered. The model takes 30 points from the past plus 17 future inputs and predicts system outputs 15 steps into the future (including the current step). Note that the number of predictions obtained by the model is the same as the length of the prediction horizon ($N = 15$), meaning that the NN needs to be called only once in the optimization problem. This helps to reduce the prediction offset caused by identifying a single-step-ahead prediction NN and calling it recursively. As for activation functions, ‘sigmoid’ and ‘swish’ were used in this work. Note that ‘sigmoid’ function leads to smooth nonlinear NN dynamics, while ‘swish’ captures steep changes better but is more aggressive at the same time.

All simulations were done in Python. Different programming libraries were employed for different model approximation methods. To be specific, MPCTools [31] was used for solving

TPWL/POD-model-based EMPC, CasADi [32] was used for solving subspace-model-based EMPC and NN-model-based EMPC. Note that the optimization solver IPOPT [33] was employed for all EMPC simulations.

4.4 Results and discussion

4.4.1 Approximation models

Six models are developed to approximate the nonlinear dynamics of the process. First, two TPWL models are developed by linearizing the original nonlinear model around 3 and 5 points respectively. Then, POD method is applied to the TPWL models, leading to two POD-TPWL models. One LTI model that takes the form of (10) is developed using the subspace identification method. The dimension of the LTI model is 2. A fully-connected NN with two hidden layers is generated. The hidden layers have 10 and 3 nodes individually.

The original model is used as the reference for performance evaluation of the approximation models. The output responses and the corresponding input trajectory of the original model and the approximation models are shown in Figure 4. The prediction performance is measured by the normalized root mean square error (NRMSE):

$$NRMSE = \frac{1}{y_s} \sqrt{\frac{\sum_{i=1}^n (\hat{y}_i - y_i)^2}{n}} \quad (16)$$

where y_s is the optimal steady-state output, n is the number of data points, \hat{y}_i is the i th output predicted by the approximation model and y_i is the i th output obtained from the original nonlinear model. The NRMSE of the approximation models are summarized in Table 1.

From Figure 4, it is observed that the TPWL and POD-TPWL models with five linearization points perform better than models with three linearization points. The application of the POD method did not impact the prediction performance significantly. Table 1 also shows consistent results. It was noticed that models perform differently with different variations in inputs. The NN model has a more noisy response compare to other models. The reason for this is that NNs are complex nonlinear functions with a significant number of parameters. Thus it is impractical to obtain the absolute optimal set of parameters, making numerical prediction errors hard to eliminate. Furthermore, it is noteworthy that NNs works with scaled variables in the range of -1 to 1, leading to more numerical errors. All the models respond to input changes without delays and converge to values that are very close to the steady-state output of the original nonlinear system when the input returns back to the steady-state value.

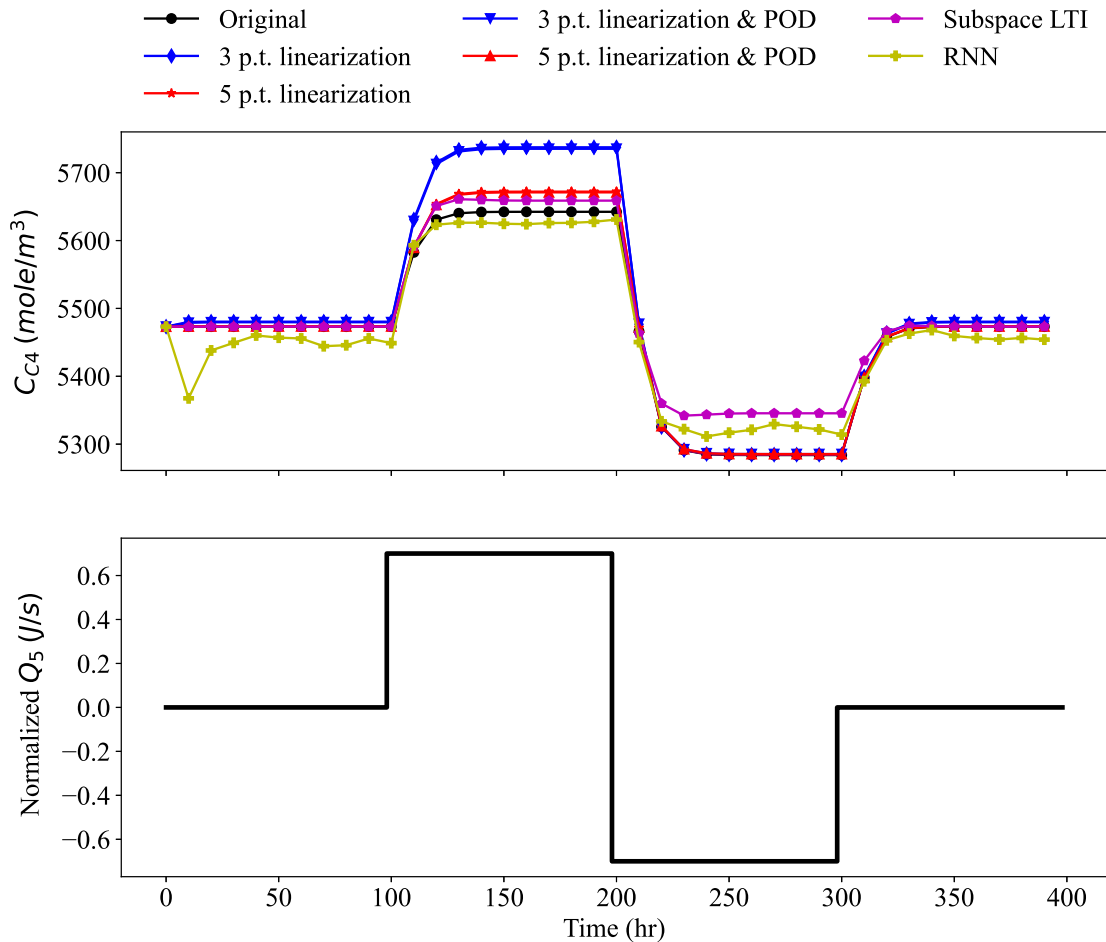


Figure 4: Open-loop output responses of the alkylation first-principle model and approximation models.

Table 1: Open-loop prediction performance of approximation models - Alkylation

Model applied	Dimension	Normalized RMSE
3 p.t. linearized	25	0.008
5 p.t. linearized	25	0.002
3 p.t. linearized & POD	15	0.008
5 p.t. linearized & POD	15	0.002
Subspace LTI	2	0.005
Neural Network	N/A	0.005

Table 2: MPC results of the original model and approximation models - Alkylation

Model applied	Dimension	Time (single step EMPC)	Objective function value
Original	25	1.16	23564.71
3 p.t. linearized	25	4.28	15619.71
5 p.t. linearized	25	2.36	22655.89
3 p.t. linearized & POD	15	0.52	46990.54
5 p.t. linearized & POD	15	0.73	48512.75
Subspace LTI	2	0.07	49933.00
Neural Network	N/A	0.27	182511.67

4.4.2 Conventional tracking model predictive control

The approximation models discussed in the previous section are employed by the MPC controller (2) with parameter settings as discussed in Section 4.2. The simulation results are summarized in Table 2. The order of the reduced model, the average time consumed in solving the MPC problem at a given time step, and the accumulated objective function value under the corresponding trajectories are presented for the considered models. Figures 5 and 6 present the tracking performance of the system output (product concentration) and the optimal control strategy of the heat supply going into CSTR-4, which is one of the manipulated inputs. The dashed black line represents the tracking set-point, while the tracking performances obtained with different approximation models are differentiated by colors and markers.

As can be observed in Table 2, TPWL models failed to improve the average computational speed for solving the optimization problem however provide satisfying tracking results. This could be caused by the complexity of the TPWL models, leading to more iterations required before the numerical solver converges to the optimal solution. The increased number of linearization points does not improve MPC controller performance. A small offset in the manipulated variable can be observed in Figure 6. Computational speed improvements were observed with model order reduction applied on top of TPWL models while the tracking performance became worse. The observation from Figure 5 matches with the results in Table 2, where slight offsets in tracking were observed for the TPWL-POD models. This is reasonable since applying model order reduction and linearization at the same time further reduces the model accuracy.

The subspace-model-based MPC provides significant computational cost reduction with an

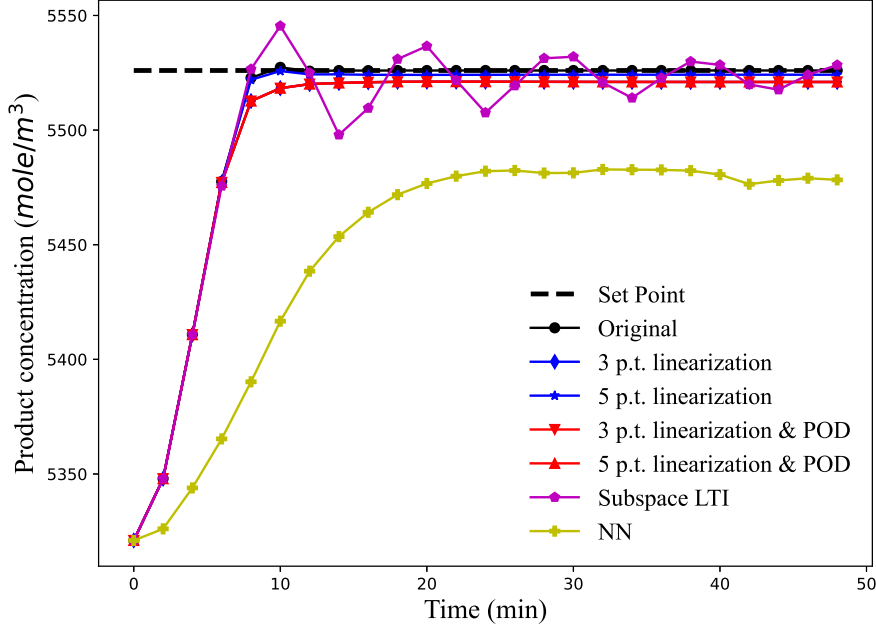


Figure 5: The optimal product concentration trajectory under different model-approximation-based conventional MPC frameworks.

under-damping response as presented in Figures 5 and 6. It is also noticed that the control strategy obtained with the subspace model changes rapidly and more aggressively. This observation is reasonable as the subspace model is linear. Compare to nonlinear models that gives predictions that are smoother and closer to the actual dynamics of the system, the linear model naturally leads to more aggressive prediction and thus more aggressive controller responses.

As for the NN model, a more significant offset was observed. The offset could be due to the input-output normalization required during training as well as prediction applications, leading to significant numerical errors. The non-smooth noisy prediction of the model also contributed to the offset. Computational cost reduction better than the first-principle-model-based models and worse than the subspace model was achieved. Note that the presented input happened to converge to the set-point for the NN model, which is not the case for all input variables.

4.4.3 Economic model predictive control

In this subsection, we study the performance of the different models in EMPC (5). The EMPC simulation results of the alkylation process are summarized in Table 3. Figure 7 presents the product concentration under the optimal control trajectory obtained under different model-approximation-based EMPC frameworks, of which an example is shown in Figure 8, where the trajectory of the

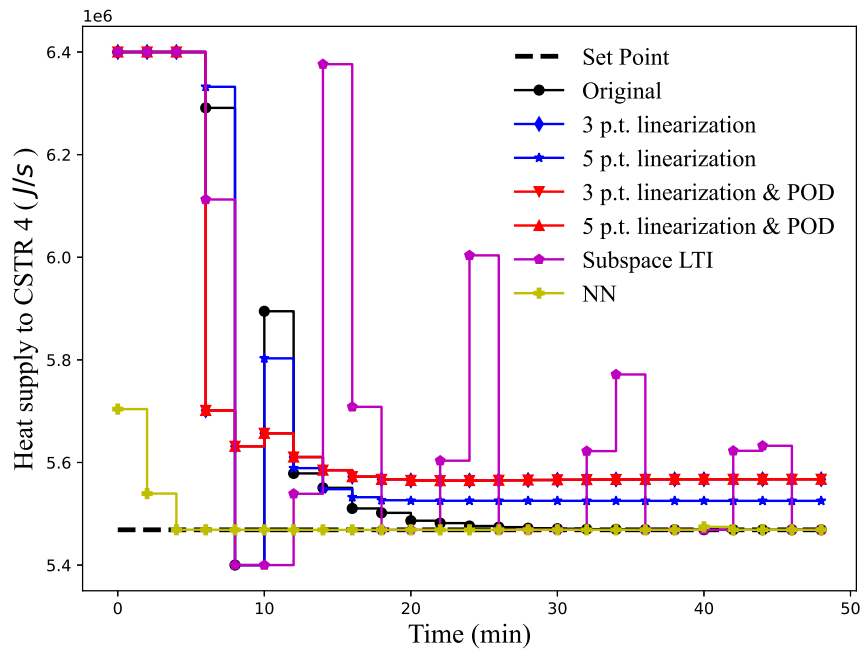


Figure 6: Manipulated input trajectory under different model-approximation-based conventional MPC frameworks - the heat supply going into CSTR-4

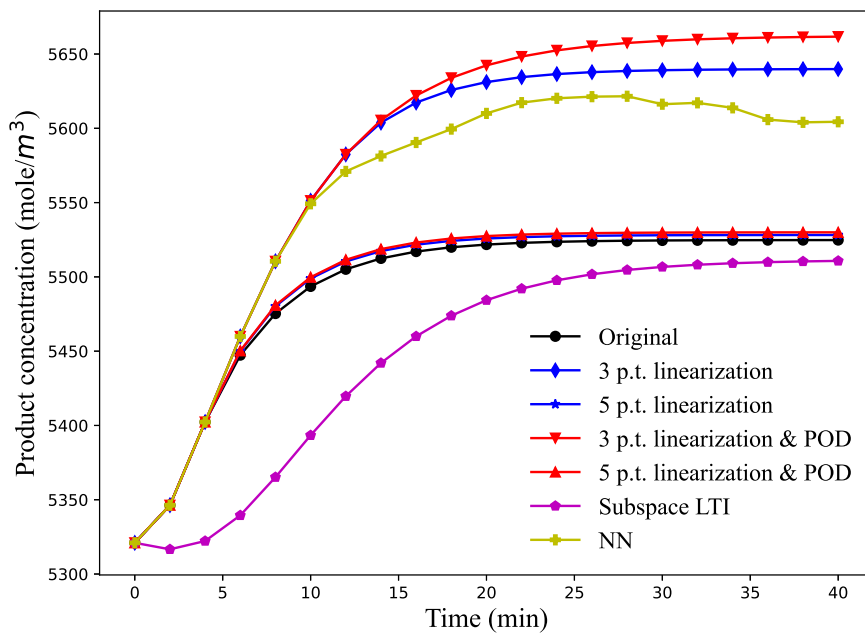


Figure 7: The optimal product concentration trajectory under different model-approximation-based EMPC frameworks.

Table 3: EMPC results of the original model and approximation models - Alkylation

Model applied	Dimension	Time (single step EMPC)	Objective function value
Original	25	0.68	-6867.40
3 p.t. linearized	25	0.67	-4244.25
5 p.t. linearized	25	0.88	-6840.55
3 p.t. linearized & POD	15	0.60	-3012.19
5 p.t. linearized & POD	15	1.39	-6825.65
Subspace LTI	2	0.06	-6739.46
Neural Network	N/A	0.52	-5396.95

heat supply for CSTR-4 is presented.

The TPWL model with 5 linearization points gives the best performance. Significant performance improvements are observed with increased linearization points regardless of the presence of model order reduction, which is different from the observation made for MPC controller design. It was also observed that the computational cost rises as the number of linearization points increases. Applying POD on top of TPWL leads to worse EMPC performance, which is similar to what has been observed in the MPC simulation results. When the reference model is relatively simple, further applying POD reduces the computational cost. The opposite is observed with increased reference model complexity (i.e when more linearization points are used). Furthermore, the performance deviates more significantly when the referencing LPV model is less accurate. Note that from Figure 7, it can be observed that if only the product concentration is considered, different conclusions regarding simulation performance will be obtained, as the heating cost index is ignored. However, it can still be observed from Figure 7 and 8 that the 5-point-TPWL model gives control strategy that is closest to that obtained with the original model.

Overall, no significant improvement in computational speed is achieved from using first-principle-model-based model reduction. The reason is that the complexity of the original system is relatively low, which can be proved by the fast computational speed while solving the EMPC problem with the original model. In the following section, it will be shown that the speed improvements with the usage of reduced models are significant for the more complex WWTP system.

As can be observed from Table 3, the computational load reduction with the subspace model employed is the highest out of all models considered. Two factors contributed to this result, namely the significant reduction in the model order and the linearity of the subspace model. A reasonable

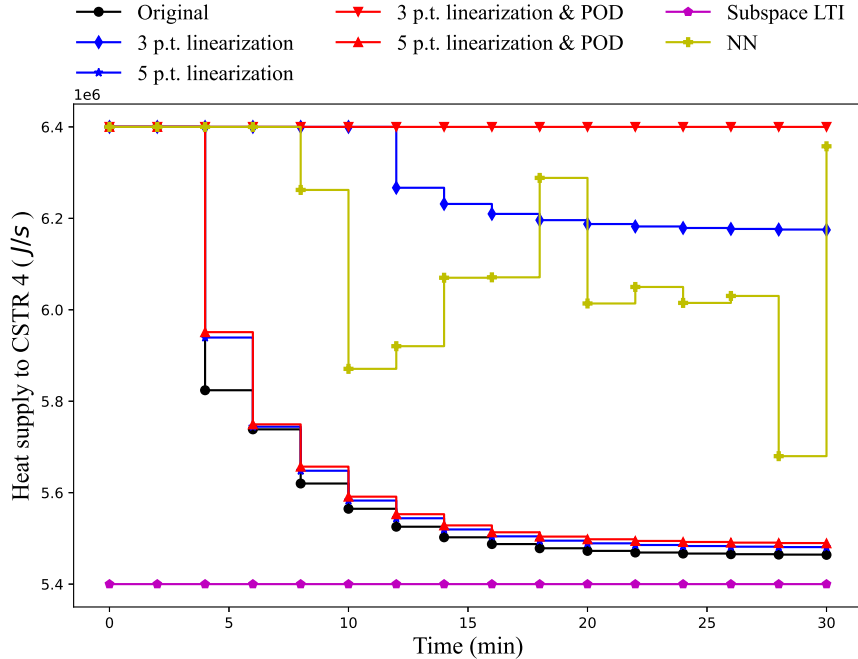


Figure 8: Manipulated input trajectory under different model-approximation-based EMPC frameworks - the heat supply going into CSTR-4

EMPC performance was also achieved with the model.

The optimal control trajectory obtained with the NN model is similar to that obtained with the models with 3 linearization points. The response is less smooth and oscillations in the control strategy can be observed from Figure 8. The improvement in computational speed achieved is slightly less than the subspace LTI model but is still quite significant. The overall performance of the NN model is better than models with 3 linearization points, but worse than models with 5 linearization points and the subspace LTI model.

5 Case Study 2: Wastewater treatment Plant

5.1 Process overview

In this section, we consider a wastewater treatment plant which is a more complex nonlinear system. A schematic of the WWTP process is shown in Figure 9. The WWTP process consists of an activated sludge bioreactor with five compartments and a secondary settler with ten layers. The reactor consists of two sections, being the non-aerated section including the first two chambers, and the aerated section which includes the latter three chambers. The wastewater stream enters the plant with a concentration Z_0 and a flow rate Q_0 . After passing through the reactor, the effluent

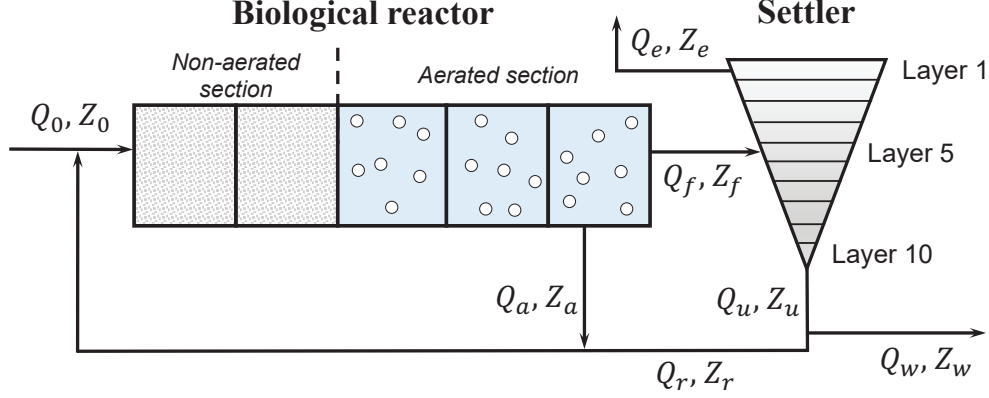


Figure 9: A schematic of the wastewater treatment plant.

is separated into two streams, in which one of them is recycled back into the first reactor chamber at flow rate Q_a and the other is fed into the settler on the fifth layer. The stream leaving from the top of the settler contains the purified water that can be disposed, while the bottom effluent is split into a recycle stream with flow rate Q_r and a waste sludge stream Q_w .

A detailed description of the dynamical model of the WWTP can be found in [28]. The model considers 8 biological reactions with 13 major compounds, including 7 soluble compounds and 6 insoluble compounds. The concentrations of the 13 compounds in each of the reactor chambers are the state variables. In the settler, a variable that represents all insoluble compounds is defined, leading to 8 states for each settler layers. The dynamical first-principle model of the WWTP consists of 145 states. Two manipulated input variables are considered, namely the oxygen transfer rate in the fifth chamber of the reactor KL_{a5} and the flow rate of the recirculation stream Q_a .

5.2 Control objective and controller setting

The economic control objective used for the EMPC controller and the steady state optimization layer of MPC are adopted from [2]. Two performance indices are considered for assessing the economic performance of the process, namely effluent quality (EQ) and overall cost index (OCI). The economic performance measure is a weighted summation of the two performance indices as follows:

$$l_e = \alpha \cdot \text{EQ} + \beta \cdot \text{OCI} \quad (17)$$

where EQ ($\text{kg pollution} \cdot \text{day}^{-1}$) is a factor that measures the processed water quality evaluated as the daily average of a weighted summation of various effluent compound concentration, OCI covers the factors that have significant impacts on the process operating cost including sludge production ($\text{kg} \cdot \text{day}^{-1}$), aeration energy ($\text{kWh} \cdot \text{day}^{-1}$), pumping energy ($\text{kWh} \cdot \text{day}^{-1}$), and mixing energy

($\text{kWh} \cdot \text{day}^{-1}$), α and β are two weighting factors for EQ and OCI, respectively. More detailed description of the cost function can be found in [2].

The system outputs are chosen to be the states required to calculate EQ and OCI. The observability of the system is validated by PBH test. In total, 41 outputs are used. However, with only 2 inputs, it is very challenging to track all 41 outputs. Thus the MPC controller is designed to track two of the outputs that deviate the most from the set-point, namely the slowly biodegradable and soluble substrate in the first and second reactor compartments. The two tracked outputs will be denoted as XS_1 and XS_2 in the following sections. The weighting parameters are defined to be $Q = \text{diag}([100, 100])$, $R = \text{diag}([100, 100])$ and $P_f = \text{diag}([1000, 1000])$. Similar to the alkylation process, the input and output vectors are only bounded:

$$\mathbb{U} = \{u \mid \underline{u} \leq u \leq \bar{u}\} \quad (18a)$$

$$\mathbb{Y} = \{y \mid y \geq 0\} \quad (18b)$$

where $\underline{u} = [0, 0]$, $\bar{u} = [240, 92230]$. Scaling is performed in implementations to reduce numerical errors.

An open-loop response of XS_1 with respect to step changes in the input vector at $t = 1 \text{ hr}$ is presented in Figure 10. The controller sampling time is 30 minutes and the prediction horizon is $N = 10$. The dynamics five hours into the future are considered by the controller, which is enough to cover the essential dynamics of the process according to Figure 10.

5.3 Data generation and model approximation

A dataset with 5376 data points (112 simulation days) is generated for the WWTP process. Samples of the training dataset are presented in Figure 11. Two output trajectories and one input trajectory are presented. Recall that XS_1 is the slowly biodegradable and soluble substrate in the first reactor compartment, Q_a is the flow rate of the recirculation stream. X_1 represents the total sludge concentration in the bottom layer of the settler. Note that the input signal is designed differently compare to the alkylation process. Instead of equally splitting the input domain, the signal is generated by adding small additional steps to a PRBS signal. This is because if the same approach is used, the complex nonlinear dynamics of the WWTP lead to an ill-conditioned dataset that can not be used for model identification. By making small changes to a working PRBS input signal, the corresponding output responses would be similar to those obtained with the PRBS signal but are able to capture the system nonlinearity. Here the small steps are added by another PRBS signal with magnitudes $[0, 0.1 \times (\bar{u}_{data} - \underline{u}_{data})]$, where \bar{u}_{data} and \underline{u}_{data} are the upper and lower bounds of

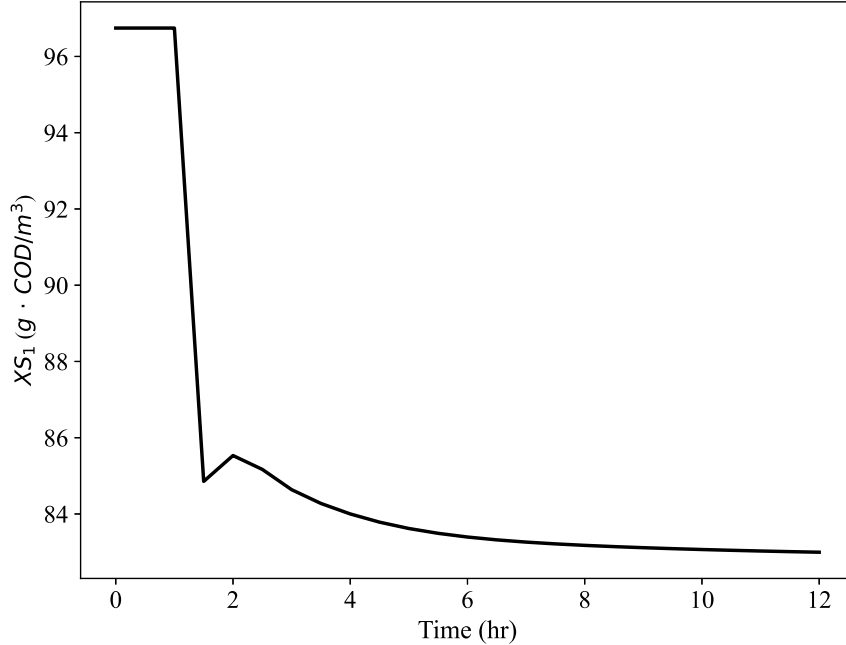


Figure 10: Step response of a WWTP process output.

the PRBS signal.

System orders of the approximation models are again determined by guess and check such that fair prediction performances are achieved. A fully-connected NN model in the following form is generated:

$$f : \mathbb{R}^{878} \rightarrow \mathbb{R}^{410}$$

where $878 = 20 \times 43 + 9 \times 2$, $410 = 10 \times 41$, 43 is the number of inputs plus outputs (2 inputs and 41 outputs), 20 is the number of past data points, 9 is the number of future inputs, 10 is the number of output steps been predicted. Again the NN is designed to fit the controller design such that the model needs to be called only once while defining the optimization problem.

5.4 Results and discussion

5.4.1 Approximation models

Six approximation models are identified for the WWTP process. Based on the original model, three sets of linearization points are investigated, namely 1, 4, and 5 linearization points. Note that due to the complexity of multi-point linearized TPWL models, simulations are not performed with TPWL models with 145 states. Instead, only TPWL-POD models with 47 artificial reduced

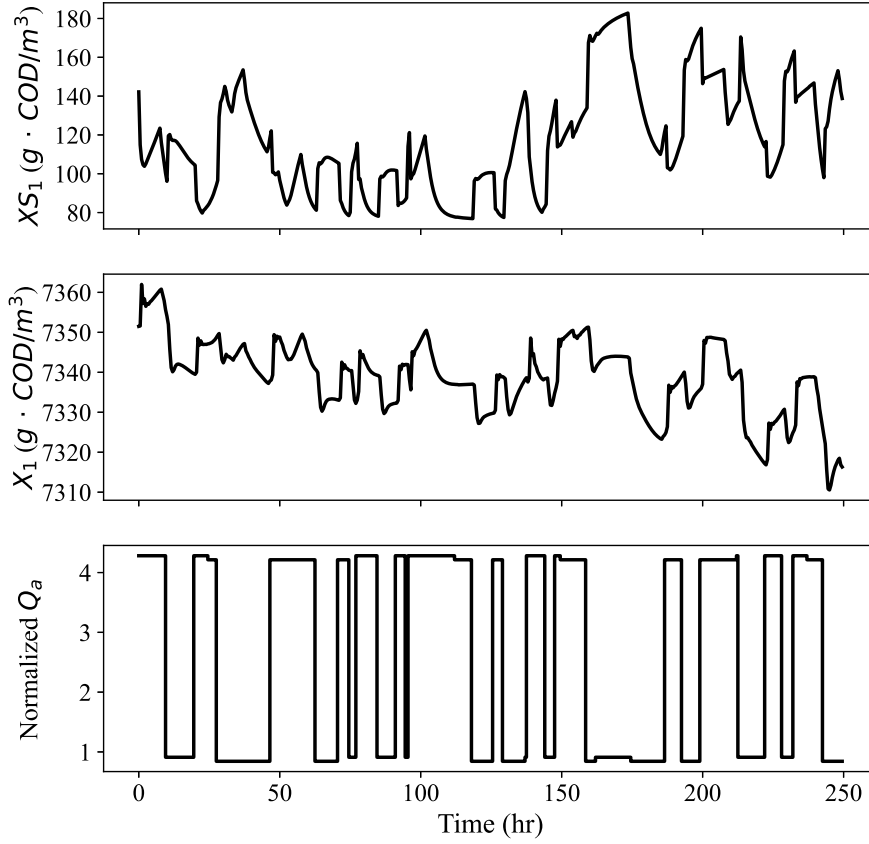


Figure 11: Multi-level input and the corresponding output response.

states are employed in MPC and EMPC simulations. An LTI model with state vector dimension $s = 48$ is identified using the subspace method. The fully-connected NN with input-output design mentioned in the previous section consists of two hidden layers, of which each layer contains 40 nodes.

Figure 12 presents the open-loop response of XS_1 and the corresponding input signal of KL_{a5} . The average RMSE of the outputs predicted by approximation models are summarized in Table 4. The application of the POD method has little effect on the open-loop prediction performance of the model with a single linearization point. As for the TPWL-POD models, the model performance improves slightly with increased linearization points. The subspace model has the worst performance due to significant information loss caused by the model linearity. The NN model performs slightly better than the subspace model as it captures the nonlinearity of the system to some extent. From Table 4, it can be concluded that the single-point-linearized model has the best prediction

Table 4: Open-loop response of the reduced model and the original model - WWTP

Model applied	Order	RMSE
1 p.t. linearized	145	0.056
1 p.t. linearized & POD	47	0.057
4 p.t. linearized & POD	47	0.059
5 p.t. linearized & POD	47	0.057
Subspace LTI	48	0.070
Neural Network	N/A	0.067

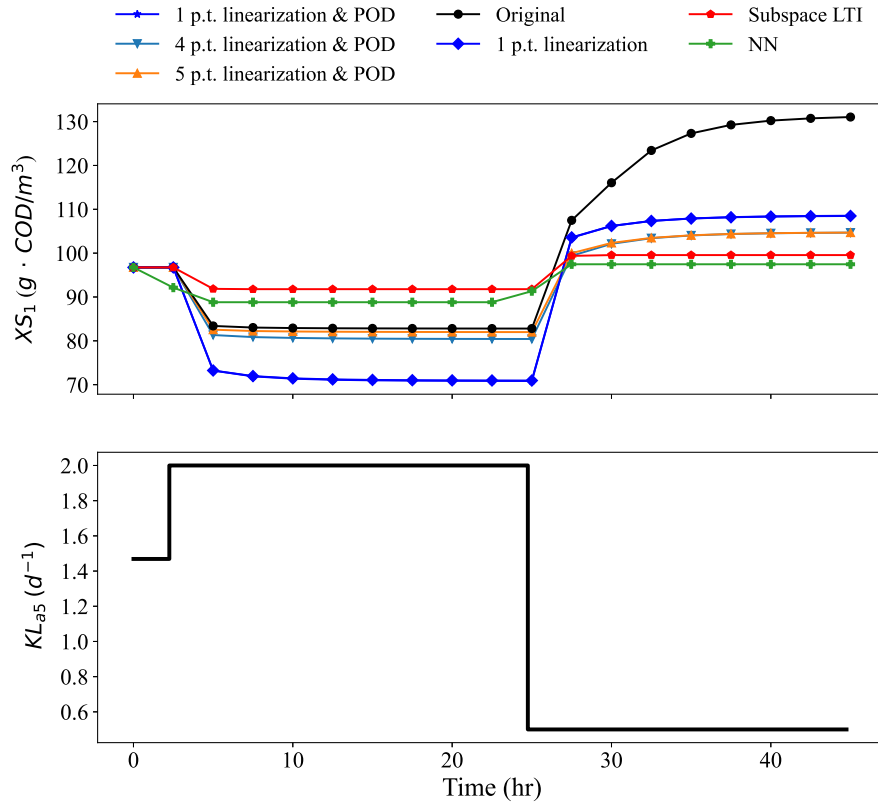


Figure 12: Open-loop output responses of the WWTP first-principle model and approximation models.

performance. To summarize, all approximation models respond to input changes without delay.

5.4.2 Conventional tracking model predictive control

MPC simulations based on the approximation models introduced in the previous section are carried out and the results are summarized in this section. Table 5 presents the average computational costs and the accumulated objective function values of the original model and the approximation models. The dynamic trajectories of XS_1 under each of the MPC controllers are shown in Figure 13, while Figure 14 presents the optimal control strategies.

As can be observed from Table 5, the single-point linearized model with reduced order converges to the set-point fastest. According to Figures 13 and 14, it also gives the optimal control strategy closest to that obtained with the original nonlinear model. Note that the model leads to the largest computational cost among first-principle-model-based approximation models, indicating the effect of the number of states considered in the optimization problem. The second fastest convergence to the set-point is given by the single-point linearized model with order reduction. A milder response in the output is also observed from Figure 13. The multi-point-linearized TPWL-POD models give similar responses, with more significant overshoots in the output at the beginning. It is also noticed that for input Q_a , the control strategies obtained based on these two models start further from the set-point. It is also observed that with an increased number of linearization points, the computational complexity increases.

Being the most efficient in terms of computational cost, the subspace model has the worst performance. A huge overshoot is observed at the beginning and it failed to converge to the set-point without offset. As shown in Figure 13, the subspace model leads to an underdamped response after the first overshooting peak. These indicate a more significant plant-model-mismatch between the subspace model and the real system. The NN model is the most computationally expensive out of all approximation models considered. This could be due to the less smooth multi-step-ahead prediction trajectory, leading to higher costs in computing Jacobian and Hessian while solving the optimization problem. It shows better performance compared to the subspace model, however offset is as well observed. Figure 14 indicates the NN model leads to an significant offset for input Q_a . To be noteworthy, the NN model is the only model that leads to an output response without overshoot in the beginning.

5.4.3 Economic model predictive control

EMPC simulations are as well performed with the approximation models and the original nonlinear model. Table 6 presents the EMPC simulation results of the WWTP process. Figure 15 shows the trajectory of the effluent quality (EQ) index under the optimal control strategies obtained with different methods, which is presented in Figure 16.

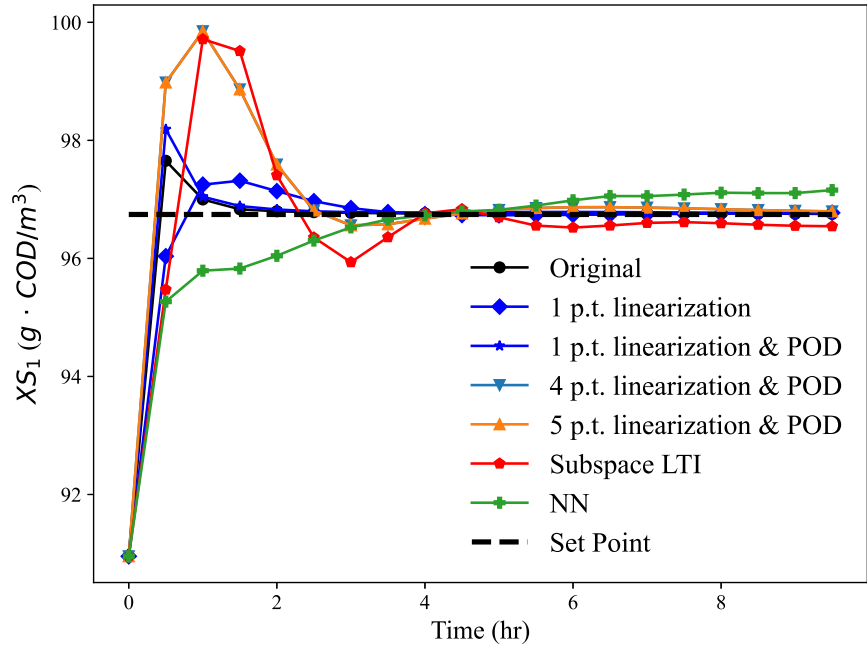


Figure 13: Optimal output trajectory of the WWTP under different model-approximation-based conventional MPC frameworks.

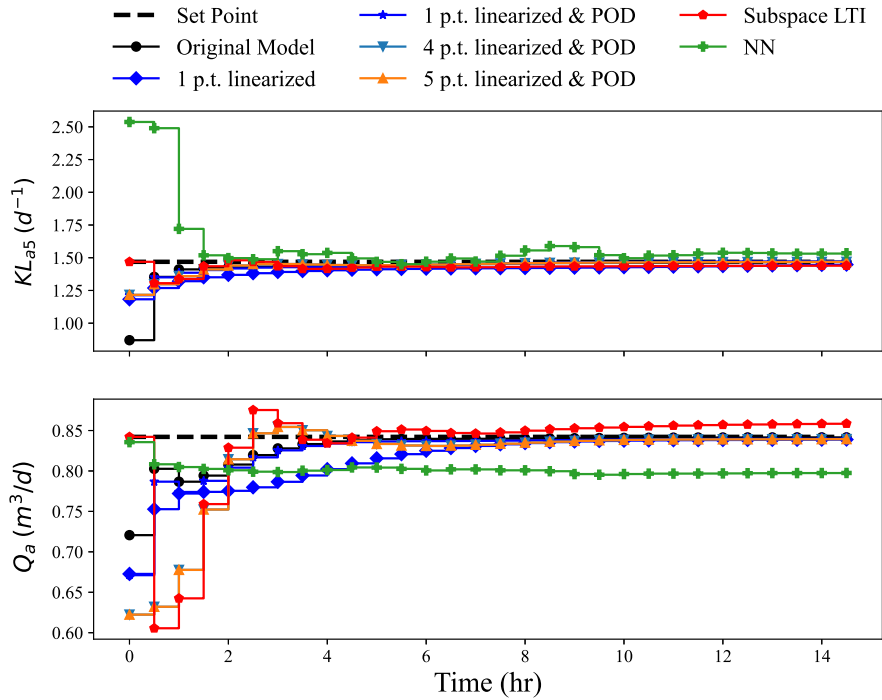


Figure 14: Optimal control policy of the WWTP under different model-approximation-based conventional MPC frameworks.

Table 5: MPC results of the reduced model and the original model - WWTP

Model applied	Order	Time	Objective
Original	145	39.63	1170.32
1 p.t. linearized	145	4.75	3891.11
1 p.t. linearized & POD	47	2.46	1403.76
4 p.t. linearized & POD	47	2.78	4736.07
5 p.t. linearized & POD	47	2.84	4736.07
Subspace LTI	48	0.48	11696.64
Neural Network	N/A	9.62	6647.17

For the first-principle-model-based model reduction, it is observed from Table 6 that the single-point linearized model has the best economic performance, which is the same as that observed in MPC simulations. With model order reduction, the computational speed was further improved however with a worse performance at the same time. The time required to solve the optimization problem increases steeply when the number of linearization points increases. The effect of model complexity is noticed to have a greater impact on EMPC compare to MPC. The economic performance however, did not improve when the number of linearization points increases. This could be because the system operates closely around the steady-state. It can be seen from Figure 15 that apart from that obtained with the original model, the best effluent quality is achieved with the single-point TPWL model. The EQ index trajectories of the multi-point TPWL-POD methods are worse and similar to each other, which matches with the results as shown in Table 6.

The subspace model leads to EMPC performances better than the multi-point linearized models but worse than the single-point linearized model. The reduction in computational cost is more significant than that achieved with the single-point linearized model as the order of the subspace models is much lower.

The NN-based EMPC framework provides economic performance slightly better than that obtained by the multi-point TPWL-POD models. The computational cost is lower than multi-point TPWL-POD models but higher than the LTI models. This is reasonable as NN is nonlinear by its nature. It is noticed from Figure 16 that the optimal control trajectory of Q_a obtained based on the NN osculates the most out of all models considered. This may be caused by the non-smooth dynamics of the NN, leading to challenges while solving the optimization problem.

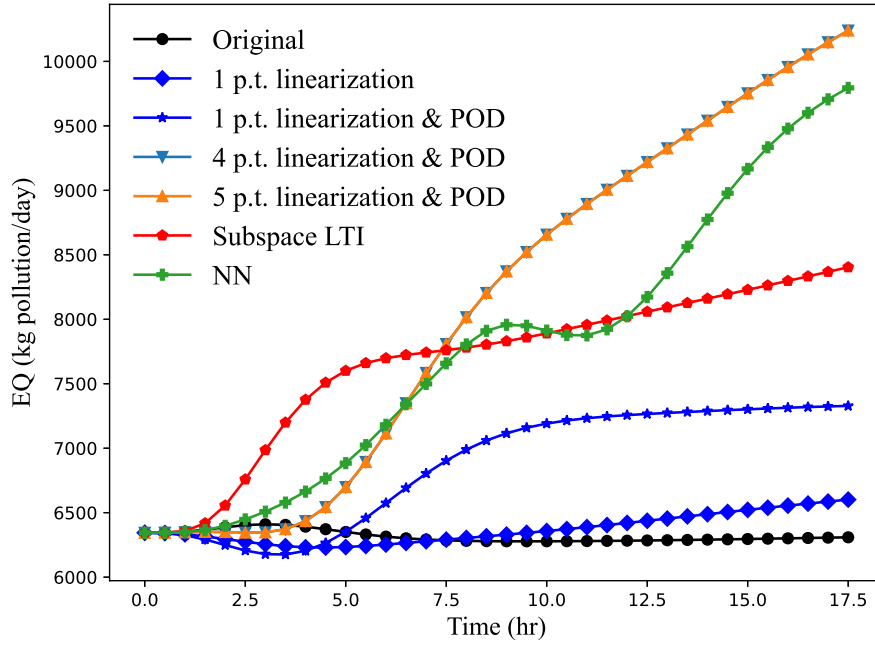


Figure 15: Effluent quality (EQ) index trajectory under different model-approximation-based EMPC frameworks.

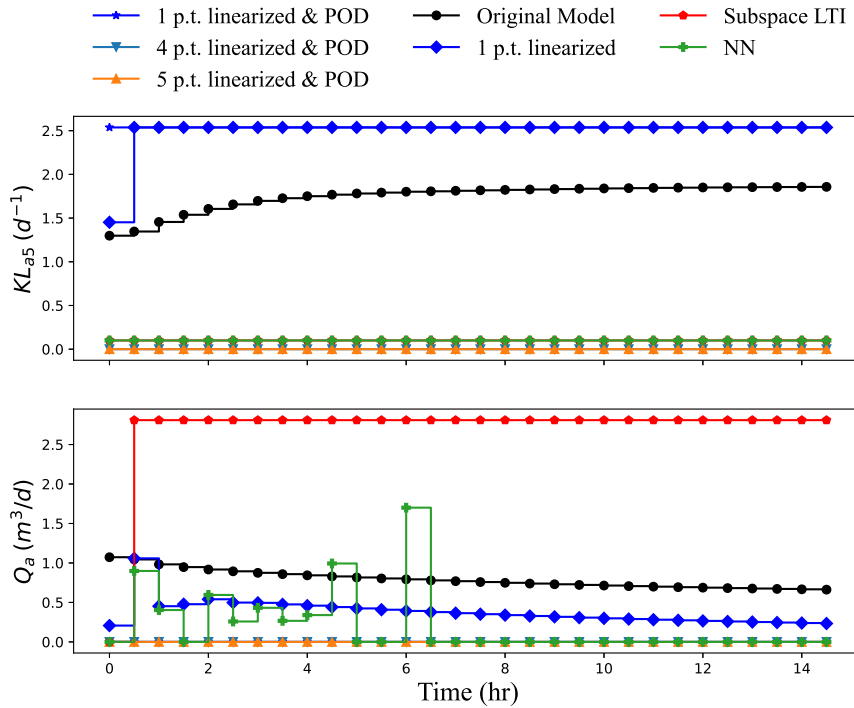


Figure 16: Optimal control trajectories under different model-approximation-based EMPC frameworks

Table 6: EMPC results of the reduced model and the original model - WWTP

Model applied	Order	Time	Objective
Original	145	396.07	115862.71
1 p.t. linearized	145	7.06	118614.70
1 p.t. linearized & POD	47	5.64	122521.16
4 p.t. linearized & POD	47	23.68	138520.05
5 p.t. linearized & POD	47	42.16	138520.05
Subspace LTI	48	6.86	121468.84
Neural Network	N/A	12.65	135274.59

6 Concluding remarks

The focus of this paper is on evaluating the applicability and performance of representative model approximation methods in MPC and EMPC. While these model approximation methods have been successful in open-loop dynamic prediction, the nature of advanced control indeed poses great challenges for these existing model approximation methods as demonstrated in the simulations of this work. We have the following conclusions and recommendations:

- Approximation models do not always lead to faster computation. The time required to do one iteration while solving the optimization problem might be reduced from using an approximation model. However, depending on the model structure, the number of iterations required might increase, resulting in a longer computational time.
- The same approximation method could perform very differently on different systems. For example, increased linearization points improve model performance for the alkylation process but not the WWTP process.
- For MPC, model accuracy and structure are essential for achieving satisfying set-point-tracking without offsets. More investigations are necessary for dataset-based approximation approaches.
- EMPC tries to track the trajectory that maximizes the economic performance. This requires the model has sufficient accuracy over the entire operating range, which poses challenges for the existing methods.

- The computational complexity of POD combined with linearization increases quickly with the increase of the number of linearization points. At the same time, the increased number of linearization points does not necessarily lead to improved control performance in the examples. How to determine the optimal number of linearization points may be a question worth further investigation.
- The NN models identified in this work focus on multi-step-ahead prediction. These models may give sufficiently accurate approximations of nonlinear systems. However, oftentimes these models return non-smooth prediction trajectories, which may pose challenges in the associated optimization. More work needs to be done to improve the overall framework. For example, an optimal operating point can be determined with NN-based EMPC first, followed by designing a more accurate controller based on the obtained set-point for better control strategies.

References

- [1] M. Ellis, J. Liu, and P. D. Christofides. Economic model predictive control: theory, formulations and chemical process applications. Springer-Verlag, London, England, 2016.
- [2] J. Zeng, and J. Liu. Economic model predictive control of wastewater treatment processes. *Industrial & Engineering Chemistry Research*, 54(21): 5710–5721, 2015.
- [3] J. Katz, B. Burnak, and E. N. Pistikopoulos. The impact of model approximation in multiparametric model predictive control. *Chemical Engineering Research and Design*, 139: 211–223, 2018.
- [4] V. B. Nguyen, S. B. Q. Tran, S. A. Khan, J.W. Rong, and J. Lou. POD-DEIM model order reduction technique for model predictive control in continuous chemical processing. *Computers & Chemical Engineering*, 133: 106638, 2020.
- [5] T. Mckelvey, H. Akcay, and L. Ljung. Subspace-based multivariable system identification from frequency response data. *IEEE Transactions on Automatic Control*, 41(7): 960–979, 1996.
- [6] F. Felici, J. W. Wingerden, M. Verhaegen. "Subspace identification of MIMOLPV systems using a periodic scheduling sequence", *Automatica*, vol. 43, pp. 1684 – 1697, 2007.
- [7] A. Zhang, J. Liu. "Economic MPC of wastewater treatment plants based on model reduction". *Processes*, vol.7, no. 10, pp. 682, 2019.

- [8] L. Zhang, D. H. Zhou, M. Y. Zhong, and Y. Q. Wang. Improved closed-loop subspace identification based on principal component analysis and prior information. *Journal of Process Control*, 80: 235–246, 2019.
- [9] S. Saki, and A. Fatehi. Neural network identification in nonlinear model predictive control for frequent and infrequent operating points using nonlinearity measure. *ISA Transactions*, 97: 216–229, 2020.
- [10] Y. G. I. Acle, F. D. Freitas, N. Martins and J. Rommes. Parameter preserving model order reduction of large sparse small-signal electromechanical stability power system models. *IEEE Transactions on Power Systems*, 34(4): 2814–2824, 2019.
- [11] S. Ibrir. A projection-based algorithm for model-order reduction with H_2 performance: A convex-optimization setting. *Automatica*, 93: 510–519, 2018.
- [12] J. Diao, J. Guo, and C. Sun. Event-triggered identification of FIR systems with binary-valued output observations. *Automatica*, 98: 95–102, 2018.
- [13] G. Liu, M. L. Yu, L. Wang, Z. Y. Yin, J. K. Liu, and Z. R. Lu. Rapid parameter identification of linear time-delay system from noisy frequency domain data. *Applied Mathematical Modelling*, 83: 736–753, 2020.
- [14] B.D.O. Anderson, J.B. Moore, R.M. Hawkes Model approximation via prediction error identification *Automatica*, 14: 615–623, 1978.
- [15] H. Akaike Maximum likelihood identification of Gaussian autoregressive moving average models *Biometrika*, 60(2): 255–265, 1973.
- [16] J. A. R. Vargas, W. Pedrycz, and E. M. Hemerly. Improved learning algorithm for two-layer neural networks for identification of nonlinear systems. *Neurocomputing*, 329: 86–96, 2019.
- [17] J. Xu, Q. H. Tao, Z. Li, X. M. Xi, J. A. K. Suykens, and S.N. Wang. Efficient hinging hyperplanes neural network and its application in nonlinear system identification. *Automatica*, 116: 108906, 2020.
- [18] E. D. Koronaki, A. M. Nikas, and A. G. Boudouvis. A data-driven reduced-order model of nonlinear processes based on diffusion maps and artificial neural networks. *Chemical Engineering Journal*, 397: 125475, 2020.

- [19] Z. Wu, D. Rincon, and P. D. Christofides. Process structure-based recurrent neural network modeling for model predictive control of nonlinear processes. *Journal of Process Control*, 89: 74–84, 2020.
- [20] Y. Zhou, S. Zheng, Z. Huang, L. Sui, Y. Chen. Explicit neural network model for predicting FRP-concrete interfacial bond strength based on a large database *Composite Structures*, 240: 111998, 2020.
- [21] X. Yin, J. Liu. State estimation of wastewater treatment plants based on model approximation. *Computers and Chemical Engineering*, 111: 79–91, 2018.
- [22] S. Tiwary and R. A. Rutenbar. On-the-fly fidelity assessment for trajectory-based circuit macromodels. *IEEE Custom Integrated Circuits Conference 2006*, 185–188, 2006.
- [23] M. Rewieński, J. White. A trajectory piecewise-linear approach to model order reduction and fast simulation of nonlinear circuits and micromachined devices. *IEEE Transactions on Computer-Aided Design of Integrated Circuits and Systems*, vol. 22, no. 2, pp. 155-170, 2003.
- [24] B. C. Csáji. Approximation with artificial neural networks. *Faculty of Sciences, Eötvös Loránd University, Hungary* 24(48): 7,2001.
- [25] Z. Wu, A. Tran, D. Rincon, P. D. Christofides. Machine learning-based predictive control of nonlinear processes. Part I: Theory, *AIChE Journal*, vol. 65, no. 11, 2019.
- [26] Z. Wu, A. Tran, D. Rincon, P. D. Christofides. Machine-learning-based predictive control of nonlinear processes. Part II: Computational implementation, *AIChE Journal*, vol. 65, no. 11, 2019.
- [27] P. D. Christofides, J. Liu, D. M. Peña. *Networked and Distributed Predictive Control - Methods and Nonlinear Process Network Applications*, Springer, 2010.
- [28] J. Alex, L. Benedetti, J. Copp, K. V. Gernaey, U. Jeppsson, I. Nopens, M. N. Pons, L. Rieger, C. Rosen, J. P. Steyer, P. Vanrolleghem, S. Winkler. Benchmark simulation model No. 1 (BSM1). *Technical Report, Department of Industrial Electrical Engineering and Automation, Lund University*, 2008
- [29] F. Chollet et al. Keras. <https://keras.io>, 2015.
- [30] M. Abadi, P. Barham, J. Chen, Z. Chen, A. Davis, J. Dean, M. Devin, S. Ghemawat, G. Irving, M. Isard, M. Kudlur, J. Levenberg, R. Monga, S. Moore, D. G. Murray, B. Steiner, P.

- Tucker, V. Vasudevan, P. Warden, M. Wicke, Y. Yu, and X. Zheng, *Google Brain*, TensorFlow: A System for Large-Scale Machine Learning, *The 12th USENIX Symposium on Operating Systems Design and Implementation (OSDI '16)*, November 2–4, 2016 • Savannah, GA, USA
- [31] M. J. Risbeck, J. B. Rawlings et al. MPCTools: Nonlinear model predictive control tools for CasADi (Python interface). <https://bitbucket.org/rawlings-group/mpc-tools-casadi>.
- [32] J. A. E. Andersson, J. Gillis, G. Horn, J. B. Rawlings, M. Diehl. "CasADi – A software framework for nonlinear optimization and optimal control". *Mathematical Programming Computation*, vol. 11, no. 1, pp. 1-36, 2019.
- [33] A. Wächter, C. Laird et al. Ipopt. <https://coin-or.github.io/Ipopt/index.html>.